Loss or mislocalization of aquaporin-4 affects diffusion properties and intermediary metabolism in gray matter of mice

T. Pavlin[1,2], E.A. Nagelhus[3], C. Brekken[1], E.M. Eyjolfsson[4], A. Thoren[3], O. Haraldseth[1], U. Sonnewald[4,5], O.P. Ottersen[3], and A.K. Håberg[4,6]

[1]Department of Circulation and Medical Imaging, Faculty of Medicine, NTNU, Trondheim, Norway

[2] Molecular Imaging Center, Department of Biomedicine, University of Bergen, Bergen, Norway

[3] Department of Molecular Medicine, Institute of Basic Medical Sciences, Faculty of Medicine, University of Oslo, Oslo

[4] Department of Neuroscience, NTNU, Trondheim, Norway

[5] Department of Drug Design and Pharmacology, Faculty of Health and Medicine, University of Copenhagen, 2100 Copenhagen, Denmark.

[6] Department of Radiology and Nuclear Medicine, St. Olavs, Trondheim University Hospital, Trondheim, Norway

Corresponding author:

Asta Kristine Håberg

Department of Neuroscience

Faculty of Medicine

Norwegian University of Science and Technology (NTNU)

7489 Trondheim, Norway

Phone: +47-90259147, Fax: +47 73551350

E-mail: asta.haberg@ntnu.no

Running title: *Diffusion and metabolism in AQP4 modified mice*

Keywords: cortex, diffusion weighted MRI, ^{13}C MRS, glutamate, glucose, membrane permeability

Conflict of interest: *The authors declare no competing financial interests or other conflicts of interests.*

Abstract

The first aim of this study was to determine how complete or perivascular loss of aquaporin-4 (AQP4) water channels affects membrane permeability for water in the mouse brain grey matter in the steady state. Time-dependent diffusion magnetic resonance imaging was performed on global *Aqp4* knock out (KO) and α-syntrophin (*α-syn)* KO mice, in the latter perivascular AQP4 are mislocalized, but still functioning. Control animals were corresponding WT mice. By combining *in vivo* diffusion measurements with the effective medium theory and previously-measured extra-cellular volume fractions, the effects of membrane permeability and extracellular volume fraction were uncoupled for *Aqp4* and *α-syn* KO. The second aim was to assess the effect of *α-syn* KO on cortical intermediary metabolism combining *in vivo* [1-^{13}C]glucose and [1,2-^{13}C]acetate injection with *ex vivo* ^{13}C MR spectroscopy. *Aqp4* KO increased the effective diffusion coefficient at long diffusion times by 5%, and a 14% decrease in membrane water permeability was estimated for *Aqp4* KO compared with WT mice. *α-syn* KO did not affect the measured diffusion parameters. In the metabolic analyses, significantly lower amounts of [4-^{13}C]glutamate and [4-^{13}C]glutamine, and percent enrichment in [4-^{13}C]glutamate were detected in the *α-syn* KO mice. [1,2-^{13}C]acetate metabolism was unaffected in *α-syn* KO, but the contribution of astrocyte derived metabolites to GABA synthesis was significantly increased. Taken together, *α-syn* KO mice appeared to have decreased neuronal glucose metabolism, partly compensated for by utilization of astrocyte derived metabolites.

Introduction

Transmembrane water transport in the brain grey matter is supported predominantly by aquaporin-4 (AQP4) water channels expressed in astrocytes and ependymocytes [1, 2]. The highest concentration of AQP4 is in astrocytic endfoot membranes abutting blood vessels, but the protein is also present in astrocytic processes in the tripartite synapse [1, 2]. AQP4 is anchored to endfoot membranes via α-syntrophin (α-syn) and other molecules in the dystrophin associated protein complex [1]. Loss of α-syn leads to redistribution of AQP4 from the perivascular endfeet to other membrane domains within the neuropil, including those facing the excitatory synapses, without altering the function of the water channel [3, 4]. AQP4 is considered to induce bulk movement of water across the brain's extracellular space (ECS) and along blood vessels, and thus also be implicated in the clearance of macromolecules from the brain parenchyma [5, 6]. The main pathophysiological role of AQP4 is induction and resolution of brain edema in response to various conditions such as brain trauma, ischemia, hemorrhage, and peri-tumor edema [2, 7]. Furthermore, changes in AQP4 expression and localization occur in epilepsy, possibly contributing to epileptogenesis and changes in seizure threshold [8-10]. In addition, autoantibodies to AQP4 are involved in the pathogenesis of neuromyelitis optica [11]. Changes in AQP4 expression or function have also been suggested to decrease clearance of extracellular macromolecules and thereby contribute to neurodegenerative diseases such as Alzheimer's disease [12]. In summary, alterations in AQP4 expression are seen across major neurological disorders, but we still lack a complete understanding of AQP4's physiological and pathophysiological functions. This study examines the role of AQP4 modifications on water diffusion measured *in vivo*, and brain intermediate metabolism *ex vivo* thereby offering new phenotypic measures of *Aqp4* knock out (KO) and *α-syn* KO mice. By implementing MRI/MRS techniques that are applicable to human research, this study also has translational potential, providing a link

between research on gene modified animals and human disorder(s) where AQP4 expression or localization is altered.

The first aim of the present study was to determine the role of AQP4 channels on water movement and thus membrane permeability, in the brain grey matter during anesthesia induced rest using time-dependent diffusion magnetic resonance imaging (dMRI) methodology and mice with either complete loss of AQP4 (global *Aqp4* KO mice) or selective removal of AQP4 from astrocytic endfeet (*α-syn* KO mice). Many of the previous magnetic resonance (MR) studies of AQP4 mediated water movement across biological barriers were *in vitro* studies relying on the paramagnetic contrast agent $MnCl_2$ [13-15]. They reported that the AQP4 channels account for 50%-66% of total water diffusion across the membrane under isotonic conditions [14, 15], which is corroborated by other *in vitro* methodology [16]. Noninvasive MR techniques such as the Filter-exchange PGSE Spectroscopy technique have also been used to investigate water movements across biological barriers [17]. Still, the far most commonly used *in vivo* technique for assessing AQP4's impact on water movement in the brain is standard diffusion weighted MRI and the resulting apparent diffusion coefficient (ADC) with or without other MR techniques added to improve the methodology [18-20]. However, although ADC is extremely sensitive to microstructural changes, it is also inherently unspecific, i.e. several microstructural changes can lead to the same change in ADC value. An improvement over the standard ADC measurement is to measure the ADC at different diffusion times and then model the time-dependence of restricted diffusion using biophysical models of tissue microstructure [21-24]. Such models describe the tissue in terms of various microstructural parameters; examples are surface-to-volume (S/V) ratio of the cells and tortuosity which can be estimated from short and long diffusion times, respectively. These measures are known to change in pathological

conditions (e.g., S/V increases with cell swelling and tortuosity increases with an increase in the extracellular space), hence any non-invasive method that has the sensitivity to detect changes in these parameters would have a great diagnostic value. To our knowledge, time-dependent dMRI has not been applied to *in-vivo* studies of water transport in animals. Based on the *in vitro* and *in vivo* literature, we hypothesized that *Aqp4* KO mice have increased ECS volume and decreased membrane permeability. In *α-syn* KO mice, on the other hand, we predicted limited effect on water movement since *α-syn* KO leads to redistribution of normally functioning AQP4 channels [3]. Our time-dependent dMRI protocol is based on a standard diffusion-weighted MRI and can easily be implemented on clinical scanners for the study of AQP4 function in human brain under normal and disease conditions [25].

The second aim of the present study was to assess cortical glucose and acetate intermediary metabolism in the awake resting state in *α-syn* KO mice using *in vivo* glucose and acetate injection and *ex vivo* ^{13}C MRS. *α-syn* KO leads to redistribution of functioning AQP4 channels from perivascular endfeet to astrocyte membranes facing excitatory synapses and other neural elements. These changes have been associated with changes in seizure threshold and increased seizure severity [3, 4, 26, 27]. Phenotyping the effect of *α-syn* KO on *in vivo* cortical glucose and acetate intermediary metabolism, provides new knowledge on the possible role of changes in neurotransmitter metabolism for the observed changes in seizure threshold and severity. The only previous study of brain metabolism in *α-syn* KO mice used ^{14}C labeled glucose and demonstrated a non- significant decrease in the levels of radioactive glucose and lactate in the brain in the baseline condition [28]. In the present study we addressed the effect of *α-syn* KO on intermediary metabolism by simultaneous *in vivo* injection of [1-^{13}C]glucose and [1,2-^{13}C]acetate in *α-syn* KO and WT mice followed by *ex vivo* analysis of cortical metabolism using MR spectroscopy (MRS), a technique that gives a

higher resolution with regard to both differentiation of metabolites and anatomical specificity than ^{14}C-based studies [29-32]. Similar methodologies can be implemented *in vivo* [33, 34].

Materials and Methods

Animals

Animal experiments were approved by and performed according to the Institutional Animal Care and Use Committee and conformed to the National Institutes of Health guidelines. Global *Aqp4* KO [35] and *α-syn* KO mice [36], both backcrossed into C57BL6/J, were used. The *AQP4* and *α-syn* KO models used in the present study do not have compensatory up- or downregulation of genes coding for other proteins involved in water and ion transport [2].

Experiment 1: Time dependent diffusion experiment for water permeability estimation

Male and female *Aqp4* KO mice (age 3–6 months) and *α-syn* KO mice (age 3–6 months) were used. Controls were male and female WT littermates. The animals received food and water *ad libitum* and kept at a light/dark cycle of 12 h, humidity 60%, temperature 22ºC.

Introduction of the theoretical and methodological background

Water movement across a biological membrane, i.e. membrane permeability, can either be driven by a net macroscopic osmotic gradient which produces a net flux of water across the membrane, or results from passive molecular diffusion during which there is no net flux of water across the membrane [37]. These two types of water movement give rise to osmotic (P_{osm}) and diffusional (P_d) membrane permeability, respectively. In pure lipid membranes, the ratio of osmotic-to-diffusional water permeability ($\Delta P_{osm}/\Delta P_d$) is equal to unity, which means that osmotic gradients do not affect the permeability of the membrane and water transport across the lipid bilayer is due to simple diffusion. On the other hand, when the

membrane contains AQP4 channels, P_{osm} will surpass P_d, and the ratio of ($\Delta P_{osm}/\Delta P_d$) will become greater than unity. This theoretical derivation is supported by results obtained in primary astrocytic cultures from *Aqp4* KO and WT mice where a 7-fold reduction in P_{osm} was present in the astrocytes from the KO group estimated with a calcein fluorescence quenching method [38]. For a general review of water permeability measurements in living cells and complex tissues using light-based imaging techniques, see Verkman [39].

NMR is an ideal technique to investigate to which extent AQP4 channels contribute to P_d under isotonic condition since NMR measures diffusional, not osmotic permeability. Several NMR studies have addressed this question *in vitro*, e.g. suspended renal proximal tubules [13], red blood cells from rodents [14] and bovina [15]. Common to these studies is the use of the paramagnetic contrast agent $MnCl_2$. $MnCl_2$ moves through potassium channels from the ECS to the intracellular space (ICS) affecting the relaxation properties of water in these spaces due to its paramagnetic properties. By measuring either the T_1 or T_2 relaxation time of water in the presence and absence of AQP4 inhibitors and then modeling the NMR signal using a two-compartment exchange model (ECS-ICS), the contribution of AQP4 channels to the P_d can be determined. It has been estimated that the contribution of AQP4 channels to P_d is best described by a channel-to-lipid water diffusional permeability ratio between 1:1 [15] to 2:1 [14]. In other words, in the cells studied, AQP4 channels accounted for between 50%-66% of total water diffusion across the membrane under isotonic conditions. These results have been corroborated recently using an ultra-high-speed line-scan coherent anti-stokes Raman scattering microscopy technique where a ~3.3 fold increase in P_d was found in cells expressing AQP4 versus cells without AQP4 [16].

One problem with using intracellular contrast agents such as $MnCl_2$ to determine P_d is the

toxicity which limits the extension of the technique to *in-vivo* studies. A safer approach is to measure water self-diffusion coefficient, which depends on the presence of barriers to diffusive motion and is directly affected by membrane permeability. Initial studies using dMRI [40] on human red blood cells modeled the diffusion signal as arising from the ECS and ICS with notably different diffusivities and exchange between the two compartments [41]. This technique allowed the determination of the exchange rate between the intra- and extracellular compartments. Most recently, the Filter-exchange PGSE Spectroscopy technique was used to measure the intracellular lifetime and the membrane permeability of baker's yeast [17]. This technique utilizes a diffusion filter that removes the signal from the molecules having a large ADC value (e.g. those in ECS) and then measures its recovery due to the water exchange with the ICS. However, to our knowledge, none of these dMRI techniques have been applied to *in-vivo* studies of water transport in animals.

In vivo dMRI studies of AQP4's impact on water movement in the brain have so far been limited to studies investigating the ADC with standard diffusion weighted MRI [18-20]. These studies demonstrated abnormal ADC values in animals where AQP4 levels have been manipulated in the baseline condition [20], and in response to pathological conditions [18, 19]. By implementing a combination of ADC mapping and T_2 relaxation times, Badaut and colleagues [20] concluded that the observed 50% decrease in the ADC values reflected changes in membrane permeability rather than in the intra-extracellular volume fractions. Although this is a reasonable interpretation, it underscores one of the main problems of standard diffusion weighted MRI; while ADC is extremely sensitive to microstructural changes, it is inherently unspecific, i.e. several microstructural changes could lead to the same change in the ADC value. An improvement over the standard ADC measurement is to measure the ADC at different diffusion times and then model the time-dependence of

diffusion using biophysical models of tissue microstructure [21-24]. In the case of restricted diffusion, the ADC will decay as a function of diffusion time as water spins encounter new barriers to diffusive motion. In the limit of zero diffusion times, the spins move freely, so the ADC approaches the free diffusion coefficient, D_0. As diffusion time increases, spins encounter progressively more barriers on their diffusive path, so the ADC decreases. Eventually, as all spins sample the characteristic length scale/dimension of the system, the ADC reaches a plateau value, $D_{eff,}$ which, together with the free diffusion coefficient, defines the tortuosity of the system, $1/T= D_{eff}/D_0$. The effective diffusion coefficient and, therefore, the tortuosity, will be affected by membrane permeability, κ, as well as the extracellular fluid volume fraction, ϕ, which defines the diffusive pathway. Therefore, by measuring D_{eff} at long diffusion times one indirectly probes changes related to κ and ϕ [22]. To further extract κ and ϕ from the diffusion signal, a theoretical model of tissue geometry is required.

The model used in this work is the effective medium theory developed by Latour et al. [22] together with previously-measured changes in extra-cellular volume fraction of *Aqp4* KO mice [42] in order to un-couple the effects of membrane permeability and extracellular volume fraction.

MRI

MRI was performed on a 7T Bruker Biospec 70/20 AS with BGA-12 400 mT/m gradients and a 72 mm volume resonator for transmit and an actively decoupled mouse brain quadrature surface coil for receive-only (Bruker Corporation, Ettlingen, Germany). ParaVision 4.0 was used for all experiments. Anesthesia was induced by isoflurane 3.5% in 67.5% N_2/32.5% O_2 in a closed chamber. During imaging, mice lay prone in a dedicated animal bed heated with circulating water, and anesthesia was delivered to the spontaneously

breathing animals through a snout mask using a small animal ventilator (Harvard Apparatus, Massachusetts, US) and maintained with 1.5-2.5% isoflurane in 67.5% N_2/32.5% O_2. Body temperature was maintained at 37±1°C, respiration at 70±10 breaths/min.

Thirty-two male and female mice (8 *Aqp4* KO and 8 WT littermates, 8 *α-syn* KO and 8 WT littermates), were included in the study of time-dependent diffusion. The MRI protocol consisted of scout scans, localized shimming using Fastmap, single-shot EPI acquisition for optimization of EPI parameters. Time-dependent diffusion measurements were obtained using diffusion-weighted single-shot echoplanar imaging pulse sequence (EPI). For diffusion times from 6.67 to 10.67 ms, a standard Stejskal-Tanner spin echo (PGSE) preparation was used (10 *b* values from 0.05 to 0.5 ms/μm^2, 3 diffusion directions, δ=4 ms, Δ=8, 9, 10, 11,12 ms), while for diffusion times from 11.17 to 148.67 ms, the stimulated spin-echo (PGSTE) preparation was used (16 *b* values from 0.05 to 0.8 ms/μm^2, 3 diffusion directions, δ=4 ms, Δ=12.5, 13, 15, 20, 50, 100, 150 ms). Imaging parameters were: TE/TR=26.15 ms/2000 ms, NEX=1, acquisition time=1min 38s (max), BW=25 kHz, FOV=20x20 mm2, matrix=84x60 as a single 2 mm thick slice.

Image analysis was performed in Matlab (R_2015b, MathWorks). A region-of-interest (ROI) was drawn in thalamus due to artifacts in cortical grey matter in some animals. To avoid partial volume effect that would contaminate the ROI with white matter structures, the ROI was positioned in a region with minimal or no diffusion anisotropy obtained from examining the diffusion signal versus *b*-value data.

Apparent diffusion coefficients (ADC) at each time point were obtained using Paravision 4.0 (Bruker Corporation, Ettlingen, Germany) by fitting a mono-exponential decay to the signal

intensity as a function of *b* value. For each diffusion time, a mean ADC and the standard error of the mean (SEM) were computed by averaging across 8 animals in each group. 95% confidence intervals were constructed for a sample size of 8 by multiplying the standard error with the factor of 2.365 instead of the commonly used factor of 2.000 because of the small sample size.

To estimate the changes in membrane permeability in *Aqp4* KO and *α-syn* KO from the time-dependent ADC measurement, we applied the theoretical framework developed by [22], which is an extension of the model proposed by [43]. In the Latour model, the diffusion coefficient at long diffusion times, $D_{eff}=\lim_{t\to\infty} D(t)$, is dependent not only on the bulk diffusion coefficient, permeability of cell membranes, and the size of restrictions (spacing between a periodic array of parallel barriers), but also on the volume fraction of ESC, which forms a connective network of diffusion pathways and is a function of the geometrical arrangement of cell membranes. The presence of ECS means that the time-dependent diffusion coefficient does not drop to zero in the limit of impermeable membranes. Instead, it approaches an asymptotic value, defined as D_{eff}. The relationship between effective diffusion, D_{eff}, membrane permeability, κ, and extracellular water fraction, ϕ, is complex and expressed by [22]:

$$\left(\frac{D_{eff}c_{eff}-D_1c_{int}}{D_{ext}c_{ext}-D_1c_{int}}\right)\left(\frac{D_{ext}c_{ext}}{D_{eff}c_{eff}}\right)^{1/3}=\phi$$

where

$$D_1c_{int}=\frac{\kappa a D_{int}c_{int}}{\kappa a+D_{int}c_{int}}$$

$$c_{eff}=\phi c_{ext}+(1-\phi)c_{int}$$

and D_{ext} and D_{int} are extra- and intracellular diffusion coefficients, c_{ext} and c_{int} are extra- and intracellular water concentrations, and a the characteristic dimension of the cell (e.g., if the cell is modeled as a sphere, then a is the radius). From the biophysical point of view, D_{eff} should be treated as the dependent variable, while κ and ϕ should be two independent variables. However, the above equation has no simple symbolic solution for D_{eff}. On the other hand, it is straightforward to rearrange the above equations to obtain an expression for κ:

$$\kappa = \frac{\phi b^{1/3} - b}{a\left(\frac{\phi b^{1/3} - 1}{D_{ext}} - \frac{\phi b^{1/3} - b}{D_{int}}\right)}$$

For simplicity, we assumed that $c_{eff}=c_{ext}=c_{int}$, and $b=D_{eff}/D_{ext}=1/T$ where T is the tortuosity of the system. This relationship allows one to compute the membrane permeability, κ, if the intra-/extracellular diffusion coefficients, extracellular volume fraction, cell dimension, and the diffusion coefficient at long diffusion times are known. The latter can be determined from the time-dependent diffusion measurements, while D_{int}, D_{ext}, ϕ, and a can be approximated from values in the literature. Alternatively, if the typical cell dimension is not known, it is straightforward to determine the relative change in membrane permeability resulting from a known change in extracellular water fraction and a known change in the effective diffusion coefficient. We assumed that $D_{ext}=2.12*10^{-5}$ cm^2/s, $D_{int}=1.56*10^{-5}$ cm^2/s [22], and that $\phi_{AQP4\ WT} = 0.2$ [42], while $D_{eff\ AQP4\ WT}$ was obtained from our time-dependent diffusion measurements and equaled approximately $0.65*10^{-5}$ cm^2/s. The change in extracellular volume fraction of *Aqp4* KO was set to 28% [42].

Since we are interested in group differences in ADC at each time point, we used an unpaired two-tail non-equal variance *t*-test at each time point. After applying the Bonferroni correction

for multiple comparisons, only *p* values <0.05/8=0.00625 were considered significant.

Experiment 2: Cortical intermediary metabolism of glucose and acetate

Animals, ^{13}C injection and cortical extraction

Six *α-syn* KO mice and 6 WT mice were used. The average mouse weight in both groups was 25 g. [1-^{13}C]glucose and [1,2-^{13}C]acetate (both 99% ^{13}C enriched) and D_2O (99.9%) were purchased from Cambridge Isotopes Laboratories (Woburn, MA, US), ethylene glycol from Merck (Darmstadt, Germany).

Animals were given an i.p. injection of [1-^{13}C]glucose (543mg/kg or 30µmoles/kg glucose; 0.3 M solution) plus [1,2-^{13}C]-acetate (504 mg/kg or 60 µmoles/kg acetate; 0.6 M solution). 15 min later animals were sacrificed using microwave fixation at 4 kW, 2.2 s (Model GA5013, Gerling Applied Engineering, California, US). The mice were decapitated and cerebral cortex was removed. Tissue samples were stored at -75°C till extraction with ice cold 0.7% perchloric acid (w/v). The tissue was homogenized by applying ultrasound using a Vibra Cell sonicator (Model VCX 750, Sonics & Materials, Newtown, CT, USA) followed by centrifugation at 4400 rpm at 4°C for 5 minutes. Supernatants were removed and pH was adjusted to 6.5-7.5 and the samples were lyophilized prior to analysis with MRS. Lyophilized samples were dissolved in 200 µl 99% D_2O with an internal standard (0.5% ethylene glycol) and pH was adjusted to values between 6.5 and 7.5. Samples were transferred into 5 mm Shigemi NMR (Shigemi Inc., Allison Park, PA, US).

MRS

Proton decoupled ^{13}C MR spectra were acquired using a BRUKER DRX-500 spectrometer (BRUKER Analytik GmbH, Rheinstetten, Germany). Spectra were recorded at 25°C with the following parameters; a 30º pulse angle and 30 kHz spectral width with 64K data points. The

number of scans was typically 10,000. The acquisition time was 1.08 s, the relaxation delay 0.5 s.

^{1}H MR spectra were acquired using the same spectrometer and with the following parameters; a 90º pulse angle and a spectral width with 32K data points, number of scans was 128. The acquisition time was 1.36 s and relaxation delay was 10 s. Water suppression was achieved by applying a low-power presaturation pulse at the water frequency.

Relevant peaks in the ^{13}C and ^{1}H spectra were identified and integrated using XWINNMR software (Bruker BioSpin, Rheinstetten, Germany). The amounts of ^{13}C labeling and the total amounts of metabolites were quantified from the integrals of the peak areas using ethylene glycol as internal standard. Correction factors for nuclear Overhauser effects and incomplete relaxation were applied to all relevant resonances in the ^{13}C spectra. Results for mono-labeled substrates were corrected for the 1.1% natural abundance of ^{13}C.

Interpretation of labeling patterns resulting from TCA cycle metabolism

Combined [1-^{13}C]glucose and [1,2-^{13}C]acetate injection allows simultaneous detection of neuronal and astrocytic metabolism, and the metabolic interactions between these cell types [44, 45]. This is due to the fact that neurons are more efficient in metabolizing glucose [46, 47] and the ability of astrocytes to convert acetate to acetyl-CoA and the absence of this process in neurons [48].

Glucose enters presumably equally both astrocytes and neurons [49], 2007, but is metabolized predominantly in the neuronal TCA cycle [50]. In neurons, label from [1-^{13}C]glucose can only be introduced into the TCA cycle as acetyl CoA via pyruvate

dehydrogenase (PDH; EC 1.2.4.1), and subsequently gives rise to [4-^{13}C]glutamate. The majority of glutamate is found in glutamatergic neurons [51]. In the astrocyte, [4-^{13}C]glutamate is either converted directly to [4-^{13}C]glutamine or reintroduced into the TCA cycle. The exchange of the aforementioned amino acids between astrocytes and neurons is called the (GABA)-glutamate-glutamine cycle. In GABAergic neurons [4-^{13}C]glutamate is rapidly converted to [2-^{13}C]GABA, and very little glutamate is present in these neurons [51]. In astrocytes [3-^{13}C]pyruvate from [1-^{13}C]glucose can enter the TCA cycle via either PDH or pyruvate carboxylase (PC, EC 6.4.1.1). Pyruvate carboxylase is the brain's principal anaplerotic enzyme [52] and is only found in astrocytes in the brain [53]. Metabolism of [1-^{13}C]glucose via PC activity gives rise to [2-^{13}C]glutamine formation in the astrocyte, which can be converted to [2-^{13}C]glutamate and [4-^{13}C]GABA in the neuronal compartments.

[1,2-^{13}C]Acetate is metabolized by acetyl CoA synthetase (EC 6.2.1.1) to [1,2-^{13}C]acetyl CoA which enters the TCA cycle in astrocytes and finally gives rise to [4,5-^{13}C]glutamate. In the astrocyte [4,5-^{13}C]glutamate is converted to [4,5-^{13}C]glutamine by the glia specific enzyme glutamine synthetase (GS, EC 6.3.1.2) [54]. Glutamate is present only in low concentrations in astrocytes [51, 55]. [4,5-^{13}C]Glutamine is released from astrocytes and taken up by neurons where glutamate is regenerated by phosphate activated glutaminase (PAG, EC 3.4.1.2) [56], which converts [4,5-^{13}C]glutamine to [4,5-^{13}C]glutamate. In GABAergic neurons [4,5-^{13}C]glutamate can be converted to [1,2-^{13}C]GABA by glutamate decarboxylase (GAD; EC 4.1.1.15). The contribution from astrocytic precursors to neuronal glutamate and GABA formation can be derived from the PC/PDH ratio, which provides an estimate of the contribution from the anaplerotic pathway (astrocytic) versus the oxidative (neuronal) in the formation of glutamate, glutamine and GABA [57]. The excess amounts of [2-^{13}C]glutamate/glutamine compared to [3-^{13}C]glutamate/glutamine are a minimum estimate of

label incorporation via PC activity compared to PDH activity in glutamate and glutamine. For GABA it is the excess labeling in [4-^{13}C]GABA compared to [3-^{13}C]GABA. Thus the PC/PDH activity was estimated for glutamine and glutamate as total amount of ^{13}C, corrected for naturally abundant ^{13}C in ([2-^{13}C]-[3-^{13}C]glutamine(glutamate))/[4-^{13}C] glutamine(glutamate), and for GABA ([4-^{13}C]-[3-^{13}C]GABA)/[2-^{13}C]GABA. Another ratio expressing the contribution from astrocytic precursors to neuronal glutamate and GABA formation is the acetate/glucose utilization ratio which is defined as amounts of [4,5-^{13}C]glutamate(glutamine)/[4-^{13}C]glutamate(glutamine), or [1,2-^{13}C]GABA/[2-^{13}C])GABA.

All NMRS results are given as mean ± SEM. Statistical comparisons were performed with an independent sampled t-test and threshold for statistical significance set to $p \leq 0.05$. Effect sizes were calculated with Cohen's *d* based on difference between two means of the two groups divided by the pooled standard deviation for the data. Cohen's *d* is often classified into small (*d*=0.15-0.40), medium (*d*=0.40-0.75), or large (*d*>0.75) effect sizes. An alternative way of interpreting Cohen's *d* is to use the measure to describe the average percentile standing between the mean of one group relative to the other group investigated. For instance, a Cohen's *d d* between 0.40-0.75 demonstrates a group difference between the 28- 44th percentile, a Cohen's *d* >0.75 is equivalent to a standing at the 45th percentile, a Cohen's *d* >1.0 at the 84th percentile, a Cohen's *d* >1.5 is at the 93rd percentile standing and a Cohen's *d* >2.0 at the 98 percentile. Statistical analyses in small groups are prone to type II errors. By including the effect size, a measure of the substantive difference, not the statistical significance of a result, is presented as well [58].

Results

Experiment 1: Time-dependent diffusion

Figure 1 shows an example of the logarithm of the MRI signal intensity (normalized to initial signal intensity) from the thalamus ROI in an *Aqp4* WT mouse as a function of *b* value. The circles show the signal decay for the shortest diffusion time (6.7 ms), while the squares show the decay for the longest diffusion time (148.7 ms). The slope of the linear fit is equal to the ADC. We clearly see from Figure 1 that the ADC at short diffusion times was smaller than the ADC at long diffusion times. This is a characteristic signature of a restricted system. Note that for $b<1$ ms/μm^2, there was no significant deviation from a mono-exponential decay, which agrees with the assumption that the diffusion was Gaussian. This condition is satisfied when $qL<<1$, where q is the area under the gradient and L is the characteristic size of the restrictions in the system. In our case, $q_{max} = 0.073$/μm, giving $L<<14$ μm. Since restrictions due to AQP4 channels are much smaller than the gradient grading of 14μm, the Gaussian phase approximation is valid. Additionally, for the diffusion process to be Gaussian two conditions have to be fulfilled. First, the diffusion distance of spins has to be bigger than the average size of the restrictions, so that spins sample a wide range of restrictions during the diffusion time. In the present study, the diffusion length was 5 μm and 20 μm for the shortest and longest diffusion time, respectively, which are both bigger than the size of restrictions. Second, the condition for fast exchange regime depends on the diffusion time. Here the longest diffusion time of approximately 150 ms is still much smaller than the predicted exchange time which is in the range of 1.25 - 2.5 sec as measured by the Flexi method [59]. Therefore, we can safely assume to be in the fast-exchange regime.

Figures 2a and 3a show time-dependent diffusion for the *Aqp4* KO and the *α-syn* KO groups, respectively, compared to the corresponding WT groups. All diffusion curves demonstrated time-dependence of ADC characteristic of a system with restriction. While unrestricted diffusion coefficient is time independent, the ADC of restricted diffusion decreases with

diffusion time and approaches an asymptotic value known as the tortuosity of the system at $t \rightarrow \infty$ ($D_{eff}/D_0 = 1/T$, where D_0 is the free-diffusion coefficient at t=0 and T is the tortuosity value). On the other hand, in the limit of zero diffusion time ($t \rightarrow 0$), the ADC approaches the free diffusion coefficient of the medium [21, 22]. However, our measured D_{eff} values showed a distinctive jump (marked by the arrow in Figure 2a and 3a) at the transition from the spin-echo to the stimulated-echo diffusion-weighted EPI pulse sequence, which was present in all animal groups. We attributed this effect to the variation of the effective diffusion gradient present in the spin-echo versus the stimulated pulse sequence, and as a consequence, we had to exclude the short diffusion-time data from our analysis.

Figures 2b and 3b show the mean D_{eff} coefficients and the 95% confidence intervals for the stimulated-echo part of the data since only the D_{eff} data from the stimulated-echo pulse sequence were used in the statistical group comparisons. The *Aqp4* KO mice have a higher mean D_{eff} coefficient compared to the *Aqp4* WT mice for all diffusion times, while the *α-syn* KO had similar D_{eff} as the corresponding WT animals. When the mean D_{eff} values for all animal groups are plotted together as in Figure 4a (error bars are omitted for clarity), the D_{eff} of both WT groups are the same within the experimental uncertainty, which is to be expected since there should be no structural differences between the two WT groups. Moreover, the D_{eff} of the *α-syn* KO group was similar to the values in both WT groups. In contrast, the depletion of AQP4 channels in the *Aqp4* KO had a statistically significant effect on D_{eff}. The *p*-value for each time point was smaller than 0.003, which is half of the *p*-value needed for 5% significance (see Methods section).

Figure 4b demonstrates that if the D_{eff} values of *Aqp4* KO were scaled by a constant factor equal to 0.955, the D_{eff} values of the *Aqp4* KO and *Aqp4* WT mice overlapped at all time

points. A similar scaling approach was used by Yao et al. [42] to show that the tortuosities of *Aqp4* KO and WT were the same, since $1/T = D_{eff}./D_0$. However, this conclusion cannot be supported by evidence in the present study due to lack of reliable short diffusion time data, which is necessary for accurate estimation of D_0.

Two-dimensional plots showing the relationship between changes in membrane permeability, effective diffusion coefficient and extracellular volume fraction based on Latour's model are presented in Figures 5a and 5b. In the simulation we assumed that $D_{ext}=2.12*10^{-5}$ cm^2/s, $D_{int}=1.56*10^{-5}$ cm^2/s [22], $\phi_{AQP4\ WT}=0.2$ [42], while $D_{eff\ AQP4\ KO}$ was obtained from the time-dependent diffusion measurements and equaled approximately $0.65*10^{-5}$ cm^2/s (Figure 2b). From these plots it is easy to see that the increase in extracellular water fraction and the decrease in the membrane permeability in the *Aqp4* KO group counteract each other. Estimations based on literature values demonstrated that if the extracellular volume fraction were to increase by 28% as measured by Yao and colleagues [42], while D_{eff} changed by 5% as measured in this work, the membrane permeability of the *Aqp4* KO would have to decrease by approximately 14%. Similarly, if the tortuosity of the two groups were unchanged (equivalent to $\Delta D_{eff}=0$ in our plot), while the extracellular volume fraction changed by 28%, the membrane permeability of *Aqp4* KO would have to decrease by approximately 24%.

<u>Experiment 2: Cortical intermediate metabolism of glucose and acetate</u>

A representative ^{13}C MR spectrum with relevant peaks is presented in Figure 6. Table 1 shows the % enrichment and total amounts of ^{13}C isotopomers of amino acid neurotransmitters and other metabolites in *α-syn* KO and WT mice. Significantly lower % enrichment was only present for [4-^{13}C]glutamate in the *α-syn* KO group. There was a trend

towards a lower % enrichment from glucose with [4-^{13}C]glutamine and [2-^{13}C]GABA, and the effect sizes of these group differences were large. Furthermore, total amounts of labeling from [1-^{13}C]glucose was significantly lower with [4-^{13}C]glutamate and [4-^{13}C]glutamine in the *α-syn* KO group, and a similar tendency was observed with [2-^{13}C]GABA also with a large effect size. There was a trend towards lower total [1-^{13}C]glucose and [3-^{13}C]lactate amounts in brain tissue of the *α-syn* KO group, with moderate large effect sizes. The enrichment with [3-^{13}C]lactate was not significantly lower in the *α-syn* KO group, but the effect size suggest lower lactate enrichment. The reduction in total [1-^{13}C]glucose amounts was on average 11.1%, while for [4-^{13}C]glutamate the reduction was on average 20.4%, for [4-^{13}C]glutamine: 26.0%, for [2-^{13}C]GABA: 19.8%, and for [3-^{13}C] lactate.: 29.3%There was no significant difference in % enrichment with or total amounts of [4,5-^{13}C]glutamate, [4,5-^{13}C]glutamine or [1,2-^{13}C]GABA, all derived from [1,2-^{13}C]acetate, between the KO and WT group, but a trend towards increased enrichment with [1,2-^{13}C]GABA and total [1,2-^{13}C]GABA was observed in the KO mice and large effect sizes were present. In the *α-syn* KO mice, significantly more [1,2-^{13}C]acetate than [1-^{13}C]glucose was used in GABA synthesis, while in glutamate and glutamine this was a trend only, with large effect sizes (Table 2). There was no significant effect of *α-syn* KO on PC/PDH ratios, but a tendency towards more PC activity was seen in glutamine (Table 2). There were no significant differences in the concentration of glutamate, glutamine, or GABA between the *α-syn* KO and WT groups (Table 3). Total amounts of lactate tended towards increased in the *α-syn* KO group compared to the WT group, with a large effect size (Table 3). The amount of succinate was somewhat reduced in the *α-syn* KO mice (Table 3). For NAA, content was similar in the two groups (Table 3).

Discussion

In the present study depletion of *Aqp4* was demonstrated to affect water movement *in vivo* in the intact animal using methodology that can also be implemented in clinical studies. *α-syn* KO, on the other hand, did not affect the measured diffusion parameters. However, *α-syn* KO reduced cortical glucose levels slightly while acetate metabolism was unaffected. A significant decrease in neuronal glutamate synthesis and increase use of astrocytic metabolites in GABA synthesis were present in *α-syn* KO mice.

Impact of Aquaporin 4 deletion or mislocalization on grey matter diffusion and water movement

In the present study *Aqp4* KO status was demonstrated to affect the self-diffusion of water as measured by dMRI. In particular, we demonstrated, for the first time, that the ADC in mouse gray matter followed diffusion-time dependence characteristic of a system with restrictions for all animal groups studied, and that *Aqp4* KO increased the effective diffusion coefficient at long diffusion times by 5%. The theoretical framework describing time-dependence of water diffusion signal that was used to interpret the data is directly applicable to biological systems, as it takes into account not only the effect of membrane permeability on the diffusion signal, but also the effect of extracellular water volume fraction [22], both of which are believed to change in the *Aqp4* KO. By using Latour's theoretical framework we were able to understand why the differences in the ADC values between the *Aqp4* KO and WT groups were small despite significant differences in membrane permeability and extracellular water volume fraction. The reason is that the two biological properties have opposing effects on the measured ADC value. An increase in the volume of the ECS results in a reduction of hindrances to water diffusion, so the ADC measured at long diffusion times (which equals D_{eff} in Latour's model [22]) will increase. On the other hand, a depletion of AQP4 channels decreases the permeability of the membrane, which leads to a more-restricted water

movement and therefore a lower ADC value. Since *Aqp4* KO mice are believed to have an increased extracellular volume fraction as well as reduced membrane permeability, the two effects together will reduce the net change in the ADC values. We believe this is a very important point that has been overlooked in previous research on the effect of AQP4 deletion or blockage on the measured diffusion signal.

The current study showed no difference in ADC between *Aqp4* WT and *α-syn* WT within the experimental error. This is expected since the two WT groups do not differ in terms of number or distribution of AQP4 protein channels [4]. These results therefore strengthen our experimental method.

The average 5% increase in the ADC in *Aqp4* KO in the current study is in stark contrast to the 50% decrease in ADC value after a 27% AQP4-specific silencing in the rodent brain under normal physiological and steady-state conditions [20]. Referring back to Figure 5, the most likely explanation for this discrepancy is an increase in the extracellular volume fraction, ϕ, in the *Aqp4* KO mice. An extracellular volume fraction increase is unlikely to occur acutely in response to silencing normal functioning AQP4. In KO models, on the other hand, there is an inborn complete loss of gene function, and adaptive and/or developmental processes may take place from conception. Indeed, significantly increased ECS in *Aqp4* KO mice has been reported using tetramethylammonium ions real-time iontophoresis [42]. Yao *et al.* [42] observed a 28% increase in the extracellular volume fraction of *Aqp4* KO mice, but could not obtain membrane permeability measures because the tetramethylammonium ions were too big to cross into cells. Our study builds upon theirs in that we are sensitive to both; permeability change as well as the change in extracellular water volume fraction. Since we cannot decouple the two with the measurement obtained, we relied on the validity and

applicability of Yao *et al.* [42]. Using the measured 28% increase in extracellular water volume fraction in *Aqp4* KO mice [42] as one of the input parameters of the Latour's model, a 14% decrease in membrane permeability of *Aqp4* KO as compared to the WT was found. If the tortuosity was unaffected in *Aqp4* KO mice, a 24% decrease in membrane permeability was found. Both these estimates of *Aqp4* KO associated changes in membrane permeability may seem very small compared to other studies, but bear in mind that this study examined change in P_d while most other measurements of permeability were performed under osmotic challenge when APQ4 will have a prominent effect.

Based on the finding that *α-syn* KO mice show a redistribution of normally functioning AQP4 channels [3, 27], we predicted that D_{eff} would be unaffected by *α-syn* status as net water diffusion through the astrocytic membrane depends on the total number of AQP4 protein channels rather than their distribution. Indeed, our time-dependent diffusion measurements were consistent with this hypothesis, as D_{eff} was similar in *α-syn* KO and WT groups. However, research has shown morphological differences between *α-syn* KO and WT groups, such as swollen astrocyte endfoot processes which might affect the value of D_{eff}. In addition, using a standard dMRI protocol at 4.7T a significant increase in ADC has been observed in *α-syn* KO compared to WT previously [26]. These discrepant findings might be explained by differences in diffusion methodologies. It is possible that the increased intracellular space of the endfoot processes, possible changes in blood-brain barrier permeability, and altered AQP4 distribution together produce no detectable net D_{eff} change.

As mentioned above, the specificity of diffusion MRI is low, in particular in complex cellular structures while Latour's model is based on a simple single cell model. Several assumptions were made in the present work to generate the relationship between D_{eff}, κ and ϕ presented in

Figure 5. For instance, we assumed that intra- and extracellular water concentrations in ICS and ECS were equal and the cell diameter unchanged in the KO compared to the WT group.

It should also be noted that it has been debated whether an accurate measurement of P_d is possible with dMRI techniques, in particular, in complex *in vivo* systems [13, 39]. According to Verkman [39], accurate measurements of P_d using NMR techniques are only possible in simple systems such as suspended red blood cells and liposomes and not in complex systems *in vivo* due to the presence of the so-called unstirred layers [60] which surround big cells and cause underestimation of P_d by several orders of magnitude. Verkman's conclusions would imply that the ADC changes resulting from AQP4 silencing [20] or AQP4 up-regulation [19], do not relate directly to changes in water permeability, but instead reflect secondary changes, such as redistribution of water between ICS and ECS, and swelling of cells. In the present study, the 5% increase in the ADC in *Aqp4* KO could result from cell swelling that was not part of our model which assumed a constant cell radius. Swelling leads to an increase in intracellular water diffusion coefficient, and if fractions of intra- and extracellular water remained approximately the same, the measured ADC would increase. In reality, the processes of cell swelling and water redistribution are not independent of each other, so the observed changes are not easy to interpret with simple models, such as Latour's model used in this study.

Our experimental design could be improved by including MRI methods that are sensitive to changes in extracellular volume fractions. For instance, one could measure the relaxation times in the presence of a contrast agent, but these techniques are invasive and not readily translatable into the clinic. A simple T_2 mapping technique could possibly be sensitive enough to changes in water distribution between the ICS and ECS, but it is time consuming

and was not part of our imaging protocol. Another option would be to obtain reliable short-time diffusion data using an oscillating-gradient spin echo diffusion sequence [61]. Sen [61] has shown that the short-time diffusion behavior depends on membrane permeability in the linear term of the time-dependent diffusion equation. It would then be possible to estimate κ from short time diffusion, and use the long-time diffusion data to determine ϕ.

Intermediary metabolism in cortex of α-syn KO mice

Glucose metabolism appeared altered in *α-syn* KO mice at rest. Mitochondrial metabolism of glucose via PDH was lower in the *α-syn* KO group as total amounts of [4-^{13}C]glutamate and [4-^{13}C]glutamine derive from [1-^{13}C]glucose metabolism were significantly reduced, and a similar tendency was present for [2-^{13}C]GABA. Moreover, % enrichment was significantly lower in [4-^{13}C]glutamate, and a trend was seen in [2-^{13}C]GABA and [4-^{13}C]glutamine. The more marked reduction of label and enrichment in [4-^{13}C]glutamate may be due to glutamate having the greatest enrichment with ^{13}C. The effect size measurements suggested that % enrichment in GABA and glutamine would have reached statistical significance if groups had been larger. Further, the somewhat lower succinate content in *α-syn* KO mice provided some additional support to the notion of reduced TCA cycle activity. There was also a slight reduction in total amounts of [1-^{13}C]glucose in cortex of *α-syn* KO compared to WT mice accompanied by a trend towards a reduction in the total amount of and enrichment in [3-^{13}C]lactate. These findings are in line with a previous study reporting slightly reduced amounts ^{14}C labeled glucose and lactate in the brains of *α-syn* KO mice in the baseline condition [28]. There is no obvious explanation of the slight reduction in cortical glucose levels, but one might speculate that astrocytic endfoot swelling observed in *α-syn* KO mice [62] may reduce glucose transport into the brain. It is impossible to rule out a systemic effect of *α-syn* KO on blood glucose levels and subsequently on cortical glucose levels, as blood

glucose was not measured in the current study where manipulation of the animals was kept to a minimum to emulate the awake, resting state. However, *α-syn* KO mice have been shown to have similar blood glucose levels as their WT counterparts [28]. Importantly, the reduction in glucose content and thereby availability, cannot fully explain the reduced amount of labelled metabolites in the current study. Indeed, the average reduction in ^{13}C labeled isotopomers was about two-threefold greater in the amino acids compared to the reduction in [1-^{13}C]glucose content, thus indicating a more significant effect of *α-syn* KO status on glucose metabolism than on glucose level in the brain. Additional evidence for a particular effect of *α-syn* KO status on glucose metabolism was provided by the reduced amount of and enrichment in [3-^{13}C]lactate combined with a trend towards significant increased lactate content. The tendency towards increased lactate level and reduction in lactate enrichment suggested lactate accumulation. Lactate accumulation may result from reduced release of lactate from the astrocytic endfeet into the perivascular space [63] in *α-syn* KO mice. Taken together *α-syn* KO appeared to affect glucose metabolism more than glucose transport into the brain, and lactate efflux may also be hindered.

On the other hand, astrocytic mitochondrial acetate metabolism was unaltered in *α-syn* KO mice, and transport of label from astrocytes to neurons in *α-syn* KO mice appeared unimpeded. There was even a significantly greater use of [4,5-^{13}C]glutamine from [1,2-^{13}C]acetate in [1,2-^{13}C]GABA synthesis in the *α-syn* KO mice. Also PC activity relative to PDH was unaffected, tending towards increased for glutamine, indicating preservation of astrocytic pyruvate metabolism via PC. Taken together, the current findings demonstrated that *α-syn* KO has heterogeneous effects on TCA cycle metabolism depending on cell type, enzymatic pathway and/or substrate.

The reduced incorporation of label from glucose and preserved to increased use of [1,2-^{13}C]acetate was accompanied by similar total glutamate, glutamine and GABA concentrations in KO and WT animals demonstrating an overall slower turnover of metabolites. Likewise, the trend towards accumulation of unlabeled lactate, accompanied by slightly reduced [3-^{13}C]lactate levels, suggested that the metabolic processes were slower in *α-syn* KO mice.

The low number of animals available reduced the statistical power and is a limitation. Based on the effect sizes, glucose metabolism was probably more affected than indicated by the significant group differences uncovered. In addition, the heterogeneous mitochondrial responses to *α-syn* KO status could have made detecting group differences more difficult. Summarized, *α-syn* KO status appeared to reduce brain glucose levels, glycolysis and utilization in the TCA cycle during the awake resting state. Such changes will impact on brain function as well as resilience, and might for instance be connected to the changes in seizure severity observed in α-*syn* KO [27].

Conclusion

Using different MR based methods the effects of *Aqp4* loss and mislocalization were explored in the present study. The results showed that water diffusion in gray matter was affected in *Aqp4* KO mice, but not *α-syn* KO mice. A redistribution of AQP4 channels did however, affect the brain's intermediary metabolism. The ADC was increased by approximately 5% in the *Aqp4* KO group compared to the litter WT group using time–dependent diffusion MRI and Latour's model of long-time diffusion behavior while the changes in intermediary metabolism in *α-syn* KO mice were specifically linked to reduced glucose metabolism via PDH.

References

1. Nielsen S, Nagelhus EA, Amiry-Moghaddam M, Bourque C, Agre P, Ottersen OP: **Specialized membrane domains for water transport in glial cells: high-resolution immunogold cytochemistry of aquaporin-4 in rat brain**. *J Neurosci* 1997, **17**(1):171-180.
2. Nagelhus EA, Ottersen OP: **Physiological roles of aquaporin-4 in brain**. *Physiol Rev* 2013, **93**(4):1543-1562.
3. Amiry-Moghaddam M, Frydenlund DS, Ottersen OP: **Anchoring of aquaporin-4 in brain: molecular mechanisms and implications for the physiology and pathophysiology of water transport**. *Neuroscience* 2004, **129**(4):999-1010.
4. Neely JD, Amiry-Moghaddam M, Ottersen OP, Froehner SC, Agre P, Adams ME: **Syntrophin-dependent expression and localization of Aquaporin-4 water channel protein**. *Proc Natl Acad Sci U S A* 2001, **98**(24):14108-14113.
5. Iliff JJ, Wang M, Liao Y, Plogg BA, Peng W, Gundersen GA, Benveniste H, Vates GE, Deane R, Goldman SA *et al*: **A paravascular pathway facilitates CSF flow through the brain parenchyma and the clearance of interstitial solutes, including amyloid β**. *Sci Transl Med* 2012, **4**(147):147ra111.
6. Xie L, Kang H, Xu Q, Chen MJ, Liao Y, Thiyagarajan M, O'Donnell J, Christensen DJ, Nicholson C, Iliff JJ *et al*: **Sleep drives metabolite clearance from the adult brain**. *Science* 2013, **342**(6156):373-377.
7. Papadopoulos MC, Verkman AS: **Aquaporin water channels in the nervous system**. *Nat Rev Neurosci* 2013, **14**(4):265-277.
8. Eid T, Lee TS, Thomas MJ, Amiry-Moghaddam M, Bjørnsen LP, Spencer DD, Agre P, Ottersen OP, de Lanerolle NC: **Loss of perivascular aquaporin 4 may underlie deficient water and K+ homeostasis in the human epileptogenic hippocampus**. *Proc Natl Acad Sci U S A* 2005, **102**(4):1193-1198.
9. Binder DK, Yao X, Zador Z, Sick TJ, Verkman AS, Manley GT: **Increased seizure duration and slowed potassium kinetics in mice lacking aquaporin-4 water channels**. *Glia* 2006, **53**(6):631-636.
10. Alvestad S, Hammer J, Hoddevik EH, Skare Ø, Sonnewald U, Amiry-Moghaddam M, Ottersen OP: **Mislocalization of AQP4 precedes chronic seizures in the kainate model of temporal lobe epilepsy**. *Epilepsy Res* 2013, **105**(1-2):30-41.
11. Hinson SR, Lennon VA, Pittock SJ: **Autoimmune AQP4 channelopathies and neuromyelitis optica spectrum disorders**. *Handb Clin Neurol* 2016, **133**:377-403.
12. Yang J, Lunde LK, Nuntagij P, Oguchi T, Camassa LM, Nilsson LN, Lannfelt L, Xu Y, Amiry-Moghaddam M, Ottersen OP *et al*: **Loss of astrocyte polarization in the tg-ArcSwe mouse model of Alzheimer's disease**. *J Alzheimers Dis* 2011, **27**(4):711-722.
13. Verkman AS, Wong KR: **Proton nuclear magnetic resonance measurement of diffusional water permeability in suspended renal proximal tubules**. *Biophys J* 1987, **51**(5):717-723.
14. Benga G, Matei H, Borza T, Poruţiu D, Lupşe C: **Comparative nuclear magnetic resonance studies on water diffusional permeability of red blood cells from mice and rats**. *Comp Biochem Physiol Comp Physiol* 1993, **104**(3):491-495.

15. Lahajnar G, Macek P, Zupancic I: **Suppression of red cell diffusional water permeability by lipophilic solutes**. *Bioelectrochemistry* 2000, **52**(2):179-185.
16. Ibata K, Takimoto S, Morisaku T, Miyawaki A, Yasui M: **Analysis of aquaporin-mediated diffusional water permeability by coherent anti-stokes Raman scattering microscopy**. *Biophys J* 2011, **101**(9):2277-2283.
17. Aslund I, Nowacka A, Nilsson M, Topgaard D: **Filter-exchange PGSE NMR determination of cell membrane permeability**. *J Magn Reson* 2009, **200**(2):291-295.
18. Meng S, Qiao M, Lin L, Del Bigio MR, Tomanek B, Tuor UI: **Correspondence of AQP4 expression and hypoxic-ischaemic brain oedema monitored by magnetic resonance imaging in the immature and juvenile rat**. *Eur J Neurosci* 2004, **19**(8):2261-2269.
19. Tourdias T, Dragonu I, Fushimi Y, Deloire MS, Boiziau C, Brochet B, Moonen C, Petry KG, Dousset V: **Aquaporin 4 correlates with apparent diffusion coefficient and hydrocephalus severity in the rat brain: a combined MRI-histological study**. *Neuroimage* 2009, **47**(2):659-666.
20. Badaut J, Ashwal S, Adami A, Tone B, Recker R, Spagnoli D, Ternon B, Obenaus A: **Brain water mobility decreases after astrocytic aquaporin-4 inhibition using RNA interference**. *J Cereb Blood Flow Metab* 2011, **31**(3):819-831.
21. Mitra PP, Sen PN, Schwartz LM: **Short-time behavior of the diffusion coefficient as a geometrical probe of porous media**. *Phys Rev B Condens Matter* 1993, **47**(14):8565-8574.
22. Latour LL, Svoboda K, Mitra PP, Sotak CH: **Time-dependent diffusion of water in a biological model system**. *Proc Natl Acad Sci U S A* 1994, **91**(4):1229-1233.
23. Novikov DS, Fieremans E, Jensen JH, Helpern JA: **Random walk with barriers**. *Nat Phys* 2011, **7**(6):508-514.
24. Novikov DS, Jensen JH, Helpern JA, Fieremans E: **Revealing mesoscopic structural universality with diffusion**. *Proc Natl Acad Sci U S A* 2014, **111**(14):5088-5093.
25. Burcaw LM, Fieremans E, Novikov DS: **Mesoscopic structure of neuronal tracts from time-dependent diffusion**. *Neuroimage* 2015, **114**:18-37.
26. Dmytrenko L, Cicanic M, Anderova M, Vorisek I, Ottersen OP, Sykova E, Vargova L: **The impact of alpha-syntrophin deletion on the changes in tissue structure and extracellular diffusion associated with cell swelling under physiological and pathological conditions**. *PLoS One* 2013, **8**(7):e68044.
27. Amiry-Moghaddam M, Williamson A, Palomba M, Eid T, de Lanerolle NC, Nagelhus EA, Adams ME, Froehner SC, Agre P, Ottersen OP: **Delayed K+ clearance associated with aquaporin-4 mislocalization: phenotypic defects in brains of alpha-syntrophin-null mice**. *Proc Natl Acad Sci U S A* 2003, **100**(23):13615-13620.
28. Cruz NF, Ball KK, Froehner SC, Adams ME, Dienel GA: **Regional registration of [6-(14)C]glucose metabolism during brain activation of α-syntrophin knockout mice**. *J Neurochem* 2013, **125**(2):247-259.
29. Haberg A, Qu H, Sonnewald U: **Glutamate and GABA metabolism in transient and permanent middle cerebral artery occlusion in rat: importance of astrocytes for neuronal survival**. *Neurochem Int* 2006, **48**(6-7):531-540.
30. Håberg A, Sonnewald U, Hammer J, Melø T, Eloqayli H: **^{13}C NMR Spectroscopy as a Toolin Neurobiology**. In: *Neural Metabolism In Vivo.* edn. Edited by Choi IY, Gruetter R: Springer; 2012.

31. Sonnewald U, Gribbestad IS, Westergaard N, Nilsen G, Unsgard G, Schousboe A, Petersen SB: **Nuclear magnetic resonance spectroscopy: biochemical evaluation of brain function in vivo and in vitro**. *Neurotoxicology* 1994, **15**(3):579-590.
32. Sonnewald U, Kondziella D: **Neuronal glial interaction in different neurological diseases studied by ex vivo 13C NMR spectroscopy**. *Nmr Biomed* 2003, **16**(6-7):424-429.
33. Öz G, DiNuzzo M, Kumar A, Moheet A, Seaquist ER: **Revisiting Glycogen Content in the Human Brain**. *Neurochem Res* 2015, **40**(12):2473-2481.
34. Roig ES, Magill AW, Donati G, Meyerspeer M, Xin L, Ipek O, Gruetter R: **A double-quadrature radiofrequency coil design for proton-decoupled carbon-13 magnetic resonance spectroscopy in humans at 7T**. *Magn Reson Med* 2015, **73**(2):894-900.
35. Thrane AS, Rappold PM, Fujita T, Torres A, Bekar LK, Takano T, Peng W, Wang F, Rangroo Thrane V, Enger R *et al*: **Critical role of aquaporin-4 (AQP4) in astrocytic Ca2+ signaling events elicited by cerebral edema**. *Proc Natl Acad Sci U S A* 2011, **108**(2):846-851.
36. Adams ME, Kramarcy N, Krall SP, Rossi SG, Rotundo RL, Sealock R, Froehner SC: **Absence of alpha-syntrophin leads to structurally aberrant neuromuscular synapses deficient in utrophin**. *J Cell Biol* 2000, **150**(6):1385-1398.
37. Parisi M, Dorr RA, Ozu M, Toriano R: **From membrane pores to aquaporins: 50 years measuring water fluxes**. *J Biol Phys* 2007, **33**(5-6):331-343.
38. Solenov E, Watanabe H, Manley GT, Verkman AS: **Sevenfold-reduced osmotic water permeability in primary astrocyte cultures from AQP-4-deficient mice, measured by a fluorescence quenching method**. *Am J Physiol Cell Physiol* 2004, **286**(2):C426-432.
39. Verkman AS: **Water permeability measurement in living cells and complex tissues**. *J Membr Biol* 2000, **173**(2):73-87.
40. Andrasko J: **Water diffusion permeability of human erythrocytes studied by a pulsed gradient NMR technique**. *Biochim Biophys Acta* 1976, **428**(2):304-311.
41. Krager J: **Zur bestimmung der diffusion in einem zweibereichsystem mit hilfe von gepulsten feldgradienten.** *Ann Phys* 1969, **479**:1–4.
42. Yao X, Hrabetová S, Nicholson C, Manley GT: **Aquaporin-4-deficient mice have increased extracellular space without tortuosity change**. *J Neurosci* 2008, **28**(21):5460-5464.
43. Crick F: **Diffusion in embryogenesis**. *Nature* 1970, **225**(5231):420-422.
44. Håberg A, Qu H, Haraldseth O, Unsgård G, Sonnewald U: **In vivo injection of [1-13C]glucose and [1,2-13C]acetate combined with ex vivo 13C nuclear magnetic resonance spectroscopy: a novel approach to the study of middle cerebral artery occlusion in the rat**. *J Cereb Blood Flow Metab* 1998, **18**(11):1223-1232.
45. Hassel B, Bachelard H, Jones P, Fonnum F, Sonnewald U: **Trafficking of amino acids between neurons and glia in vivo. Effects of inhibition of glial metabolism by fluoroacetate**. *J Cereb Blood Flow Metab* 1997, **17**(11):1230-1238.
46. Lundgaard I, Li B, Xie L, Kang H, Sanggaard S, Haswell JD, Sun W, Goldman S, Blekot S, Nielsen M *et al*: **Direct neuronal glucose uptake Heralds activity-dependent increases in cerebral metabolism**. *Nat Commun* 2015, **6**:6807.

47. Qu H, Haberg A, Haraldseth O, Unsgard G, Sonnewald U: **(13)C MR spectroscopy study of lactate as substrate for rat brain**. *Dev Neurosci* 2000, **22**(5-6):429-436.
48. Sonnewald U, Westergaard N, Schousboe A, Svendsen JS, Unsgård G, Petersen SB: **Direct demonstration by [13C]NMR spectroscopy that glutamine from astrocytes is a precursor for GABA synthesis in neurons**. *Neurochemistry International* 1993, **22**(1):19-29.
49. Nehlig A, Coles JA: **Cellular pathways of energy metabolism in the brain: is glucose used by neurons or astrocytes?** *Glia* 2007, **55**(12):1238-1250.
50. Qu H, Håberg A, Haraldseth O, Unsgård G, Sonnewald U: **(13)C MR spectroscopy study of lactate as substrate for rat brain**. *Dev Neurosci* 2000, **22**(5-6):429-436.
51. Ottersen OP: **Postembedding immunogold labelling of fixed glutamate: an electron microscopic analysis of the relationship between gold particle density and antigen concentration**. *J Chem Neuroanat* 1989, **2**(1):57-66.
52. Patel MS: **The relative significance of CO2-fixing enzymes in the metabolism of rat brain**. *J Neurochem* 1974, **22**(5):717-724.
53. Yu AC, Drejer J, Hertz L, Schousboe A: **Pyruvate carboxylase activity in primary cultures of astrocytes and neurons**. *J Neurochem* 1983, **41**(5):1484-1487.
54. Norenberg MD, Martinez-Hernandez A: **Fine structural localization of glutamine synthetase in astrocytes of rat brain**. *Brain Res* 1979, **161**(2):303-310.
55. Ottersen OP, Zhang N, Walberg F: **Metabolic compartmentation of glutamate and glutamine: morphological evidence obtained by quantitative immunocytochemistry in rat cerebellum**. *Neuroscience* 1992, **46**(3):519-534.
56. Kvamme E, Torgner IA, Roberg B: **Kinetics and localization of brain phosphate activated glutaminase**. *J Neurosci Res* 2001, **66**(5):951-958.
57. Taylor A, McLean M, Morris P, Bachelard H: **Approaches to studies on neuronal/glial relationships by 13C-MRS analysis**. *Dev Neurosci* 1996, **18**(5-6):434-442.
58. Sullivan GM, Feinn R: **Using Effect Size-or Why the P Value Is Not Enough**. *J Grad Med Educ* 2012, **4**(3):279-282.
59. Nilsson M, van Westen D, Ståhlberg F, Sundgren PC, Lätt J: **The role of tissue microstructure and water exchange in biophysical modelling of diffusion in white matter**. *MAGMA* 2013, **26**(4):345-370.
60. Barry PH, Diamond JM: **Effects of unstirred layers on membrane phenomena**. *Physiol Rev* 1984, **64**(3):763-872.
61. Sen P: **Time-dependent diffusion coefficient as a probe of the permeability of the pore wall**. *J Chem Phys* 2003, **119**(18):9871-9876.
62. Amiry-Moghaddam M, Otsuka T, Hurn PD, Traystman RJ, Haug FM, Froehner SC, Adams ME, Neely JD, Agre P, Ottersen OP *et al*: **An alpha-syntrophin-dependent pool of AQP4 in astroglial end-feet confers bidirectional water flow between blood and brain**. *Proc Natl Acad Sci U S A* 2003, **100**(4):2106-2111.
63. Gandhi GK, Cruz NF, Ball KK, Dienel GA: **Astrocytes are poised for lactate trafficking and release from activated brain and for supply of glucose to neurons**. *J Neurochem* 2009, **111**(2):522-536.

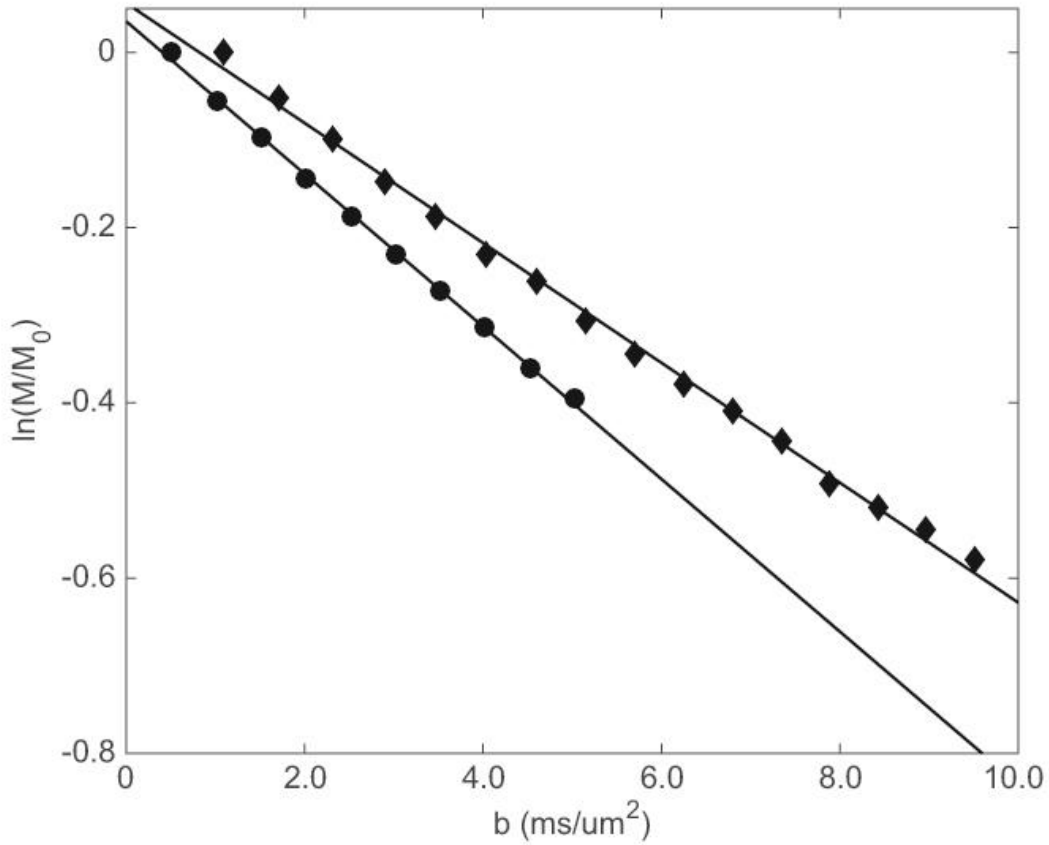

Figure 1. The MRI signal as a function of *b* for the shortest (6.7 ms, *circles*) and longest (148.7 ms, *squares*) diffusion times in a representative *Aqp4* KO mouse and the mono-exponential fits to the data.

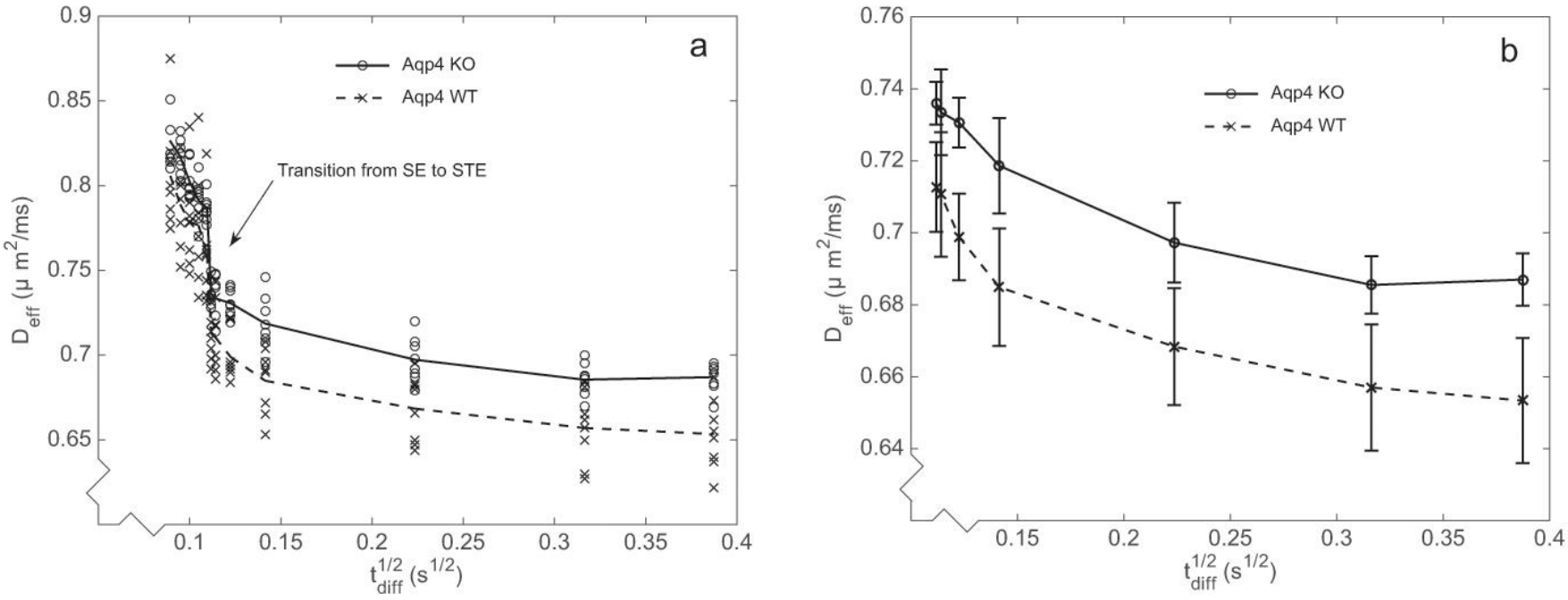

Figure 2. Time-dependent diffusion (in μm^2/ms) for *Aqp4* KO mice (*solid curve*, *circles*) compared to corresponding WT animals (*interrupted curve*, *crosses*). **a)** *Scatter plot* of $\boldsymbol{D}_{eff}$ as a function of time for all diffusion times used in the time-dependent diffusion experiment. ***b)*** Mean $\mathbf{D}_{eff}$ with 95% confidence interval for the diffusion times obtained with the stimulated-echo diffusion-weighted single-shot EPI.

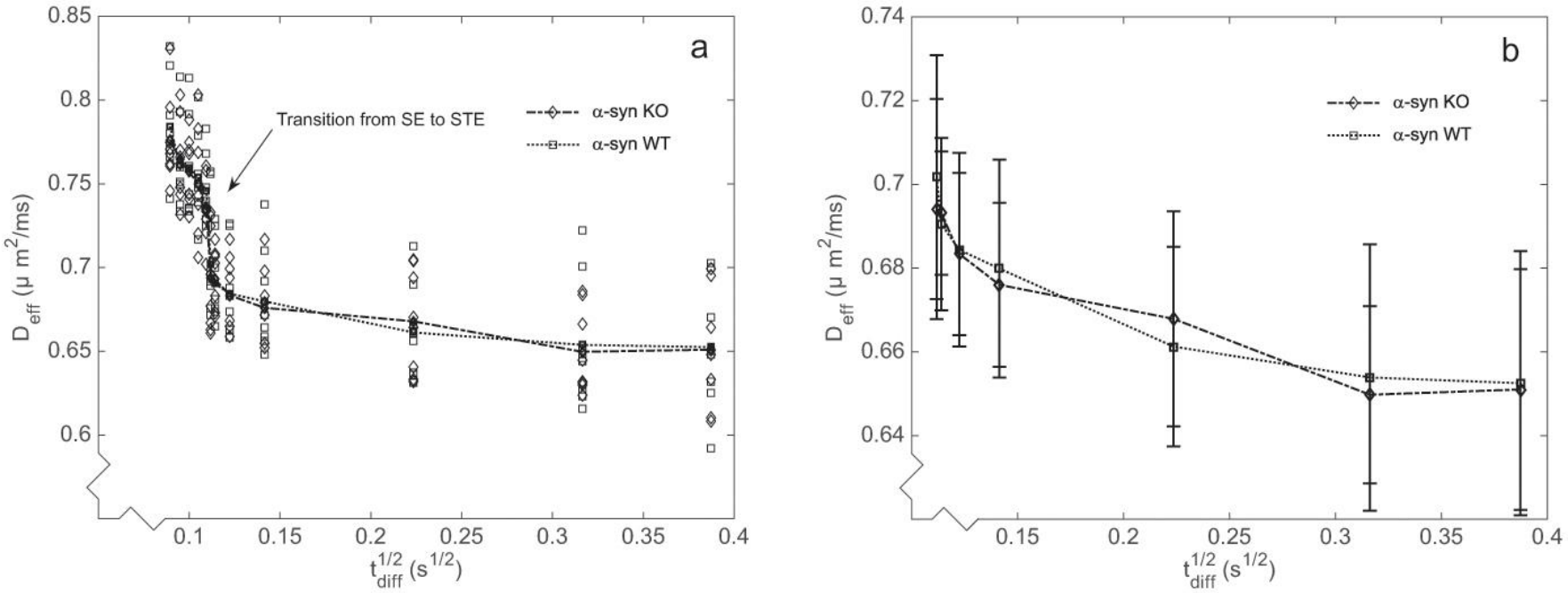

Figure 3. Time-dependent diffusion (in μm^2/ms) for *α-syn* KO mice (*interrupted-dot curve*, *diamonds*) compared to corresponding WT animals (*dot curve*, *squares*. a) *Scatter plot* of $\boldsymbol{D}_{eff}$ as a function of time for all diffusion times used in the time-dependent diffusion experiment.)*b* Mean $\mathbf{D}_{eff}$ with 95% confidence interval for the diffusion times obtained with the stimulated-echo diffusion-weighted single-shot EPI.

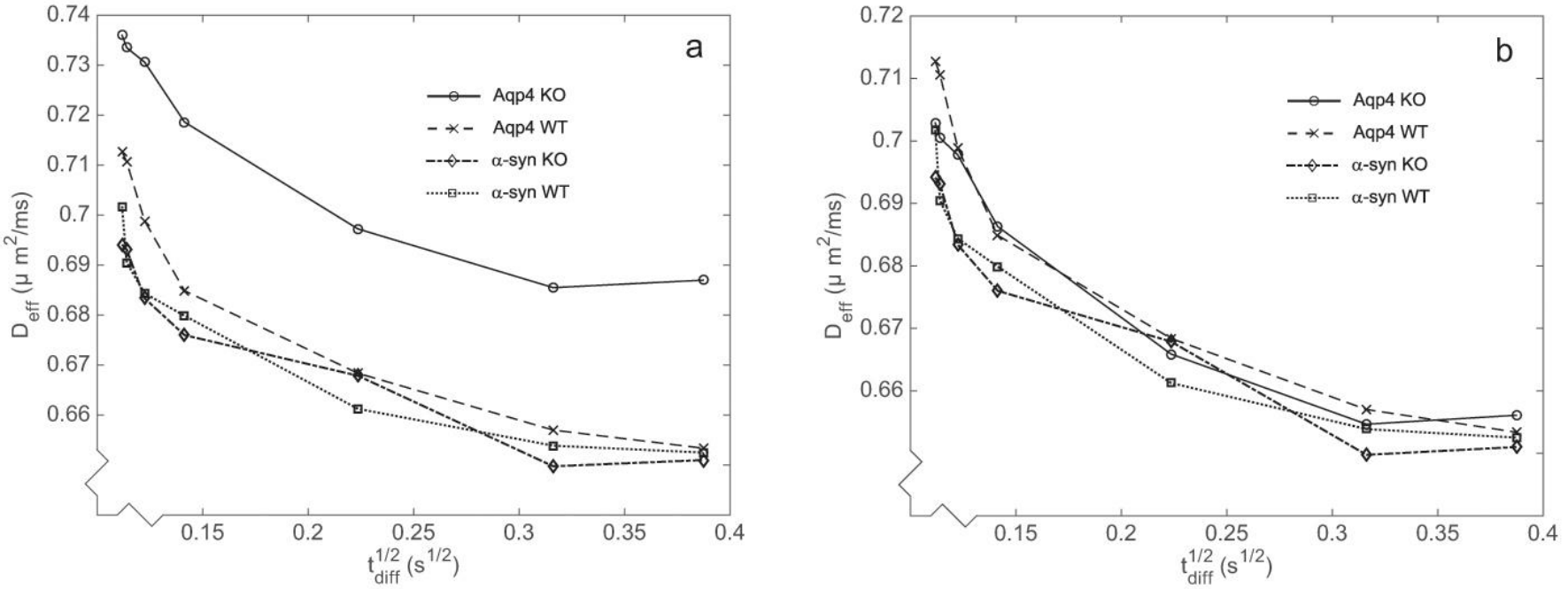

Figure 4. **T**ime-dependent diffusion (in μm^2/ms) for all animal groups: *Aqp4* KO (*solid curve*, *circles*), *Aqp4* WT (*interrupted curve*, *crosses*), *α-syn* KO (*interrupted-dot curve*, *diamonds*), *α-syn* WT (*dot curve*, *squares*). **a**) Mean $\boldsymbol{D}_{\text{eff}}$ as a function of time for all animal groups used in the experiment. ***b)*** Same as left, except that the $\mathbf{D}_{\text{eff}}$ of the Aqp4 KO group has been scaled by a factor of 0.955 to match the mean **D** eff values of the other groups.

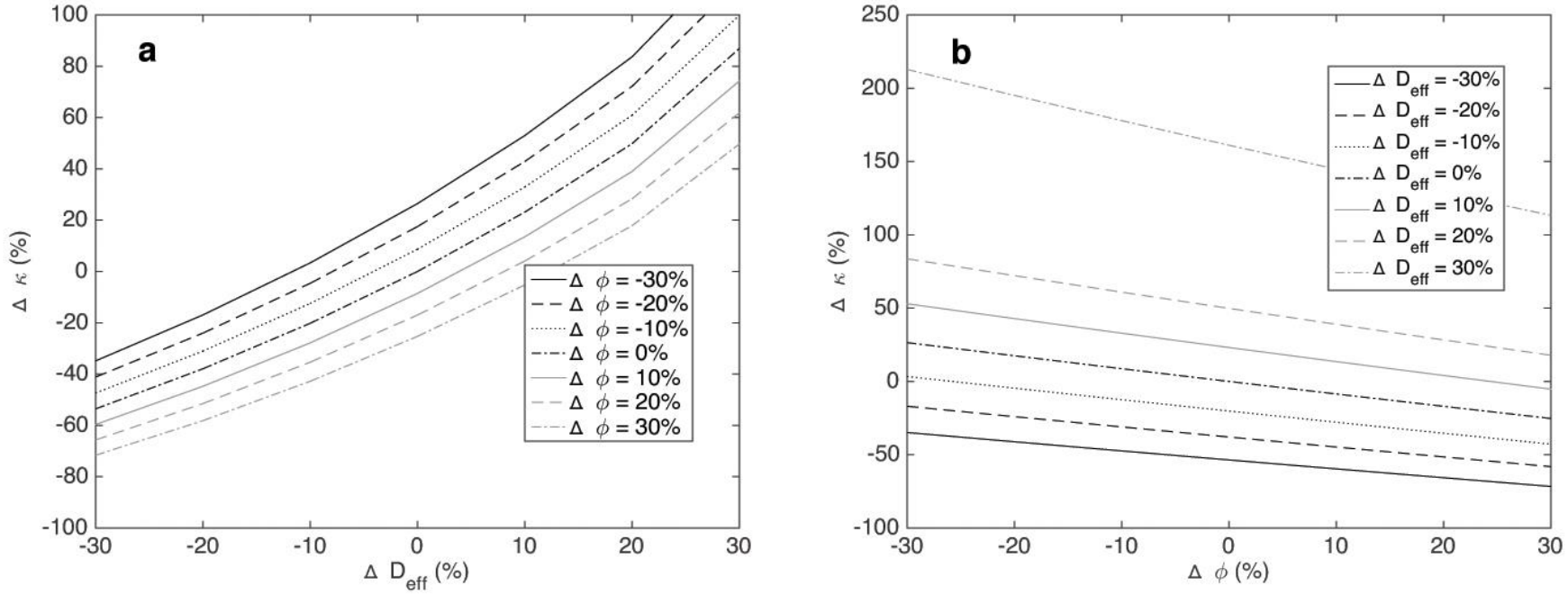

Figure 5. Percent changes in κ due to changes in Φ and $\mathbf{D}_{eff}$. **a)** Δκ as a function of $\Delta\mathbf{D}_{eff}$ for a range of discrete Φ values. **B)** Δκ as a function of $\Delta\Phi$ for a range of discrete $\Delta\mathbf{D}_{eff}$ values.

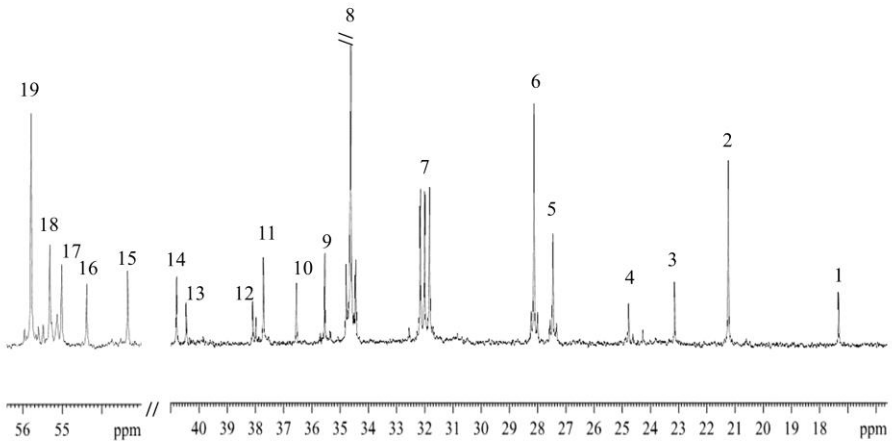

Figure 6. Ex vivo 13C MRS of cortical extract of a *α-syn* WT mouse injected with [1-^{13}C]glucose and [1,2-^{13}C]acetate (for details see Materials and methods). The singlets are monolabeled metabolites predominantly derived from [1-^{13}C]glucose metabolism, whereas doublets are double-labeled (in consecutive positions) metabolites mainly originating from [1,2-13C]acetate metabolism. Peak assignment: *1* alanine C3, *2*

lactate C3, *3N*-acetylaspartate C6, *4* GABA C3, *5* glutamine C3, *6* glutamate C3, *7* glutamine C4, *8* glutamate C4, *9* GABA C2, *10* taurine C2, *11* aspartate C2, *12* creatine C4, *13* GABA-4, 14 *N*-acetylaspartate C2, *15* aspartate C2, 14 *N*-acetylaspartate C2, *17* creatine C4, *18* glutamine C2, *19* glutamate C2. *Parallel lines* indicate that peak is truncated.

Table 1. Percent enrichment and total amounts of ^{13}C (mean± SEM) in amino acids and lactate in cortex of α-syntrophin (*α-syn*) wild type (WT) (n=6) and knock out (KO) mice (n=6) after *in vivo* intraperitoneal injection of [1-^{13}C]glucose and [1,2-^{13}C]acetate and subsequent *ex vivo* ^{13}C and ^{1}H NMRS analyses of extracts.

	Percent enrichment with ^{13}C labelled metabolite				Total amounts of ^{13}C (nmol/g tissue)			
Metabolite	***α-syn* WT**	***α-syn* KO**	***p*-value**	**Cohen's *d***	***α-syn* WT**	***α-syn* KO**	***p*-value**	**Cohen's *d***
[4-^{13}C]Glutamate	9.23±0.49	7.10±0.82*	**0.02**	1.63	1076.6 ± 40.6	856.5 ± 51.8*	**0.01**	2.12
[4-^{13}C]Glutamine	3.45±0.18	2.45±0.62	0.21	1.10	215.8 ± 12.2	158.7 ± 13.5*	**0.02**	1.99
[2-^{13}C]GABA	7.24±1.00	5.83±0.34	0.29	1.89	119.3 ± 10.3	95.6 ± 3.4	0.07	1.38
[4,5-^{13}C]Glutamate	1.18±0.16	1.19±0.11	0.97	0.04	122.8 ± 13.0	122.7 ± 7.4	0.49	0.00
[4,5-^{13}C]Glutamine	2.77±0.52	2.53±0.43	0.74	0.27	126.8 ± 10.1	114.8 ± 4.3	0.23	0.69
[1,2-^{13}C]GABA	1.89±0.34	3.16±0.57	0.15	1.65	39.7 ± 0.8	47.2 ± 4.8	0.26	0.96
[3-^{13}C]Lactate	10.53±2.40	7.44±2.42	0.17	1.28	187.1 ± 3.5	1667.0 ± 13.4	0.30	0.90
[1-^{13}C]Glucose	NA	NA			393.1 ± 18.8	349.5 ± 22.6	0.12	0.94

Statistical comparisons were performed with an independent sample T test, $p \leq 0.05$ was considered significant. Cohen's *d* was calculated as a measure of effect size. For details see Materials and Methods section. NA, not applicable.

1

Table 2. Metabolic contribution from astrocytes to neurons as derived from the Pyruvate Carboxylase (PC) versus Pyruvate Dehydrogenase (PDH) ratio and the Acetate (A) versus Glucose (G) ratio (mean± SEM) in cortex in α-syntrophin (*α-syn*) wild type (WT) (n=6) and knock out (KO) mice (n=6).

	Glutamate		**Glutamine**		**GABA**	
	A/G ratio	*PC/PHD ratio*	*A/G ratio*	*PC/PHD ratio*	*A/G ratio*	*PC/PHD ratio*
***α-syn* WT**	0.13 ± 0.04	0.18 ± 0.01	0.79 ± 0.20	0.48 ± 0.06	0.45 ± 0.05	NA
***α-syn* KO**	0.17 ± 0.02	0.17 ± 0.02	1.02 ± 0.14	0.58 ± 0.12	0.66 ± 0.13*	NA
***p*-value**	0.11	0.18	0.10	0.13	**0.05**	-
Cohen's *d*	1.26	0.63	1.33	1.05	2.13	-

For details on the metabolic ratios see Methods.

Statistical comparisons were performed with independent sample T test, $p \leq 0.05$ was considered significant.

Cohen's *d* calculated as a measure of effect size, for details see Materials and Methods section.

NA, not applicable as labeling in [4-^{13}C] GABA was not present in reliable amounts.

Table 3. Total amounts of metabolites (mean± SEM) in cortex in α-syntrophin (*α-syn*) wild type (WT) (n=6) and knock out (KO) mice (n=6)

	Total amounts of metabolites in μmol/g			
Metabolite	***α-syn* WT**	***α-syn* KO**	***p*-value**	**Cohen's *d***
Glutamate	10.44 ± 0.34	10.25 ± 0.46	0.33	0.22
Glutamine	4.58 ± 0.30	4.63 ± 0.82	0.46	0.03
GABA	1.64 ± 0.11	1.60 ± 0.06	0.43	0.21
NAA	6.69 ± 0.20	6.75 ± 0.32	0.45	0.11
Succinate	0.31 ± 0.02	0.27 ± 0.03	0.19	0.72
Lactate	1.80 ± 0.24	2.26 ± 0.12	0.07	1.07

Amounts of metabolites were measured in brain tissue extracts using ^{1}H MRS.

For details see Material and Methods section.

Statistical comparisons were performed with independent sample T test, $p \leq 0.05$ was considered significant.

Cohen's *d* calculated as a measure of effect size for details see Material and Methods section. NAA; N-acetyl-aspartate.

1

1

1